Applied Catalysis B: Environmental 100 (2010) 245–253

Contents lists available at ScienceDirect

Applied Catalysis B: Environmental

journal homepage: www.elsevier.com/locate/apcatb

Ni-decorated carbon nanotube-promoted Ni–Mo–K catalyst for highly efficient synthesis of higher alcohols from syngas

Chun-Hui Ma[a], Hai-Yan Li[a], Guo-Dong Lin[a], Hong-Bin Zhang[a,b,*]

[a] Department of Chemistry, College of Chemistry and Chemical Engineering, Xiamen University, Xiamen 361005, China
[b] State Key Laboratory of Physical Chemistry for Solid Surfaces and National Engineering Laboratory for Green Chemical Productions of Alcohols-Ethers-Esters, Xiamen University, Xiamen 361005, China

ARTICLE INFO

Article history:
Received 12 April 2010
Received in revised form 18 July 2010
Accepted 31 July 2010
Available online 7 August 2010

Keywords:
Higher alcohol synthesis
Multi-walled carbon nanotubes
Ni-decorated MWCNTs
x% Ni/CNT-doped Ni–Mo–K catalyst

ABSTRACT

A type of metallic nickel-decorated CNT-doped Ni–Mo–K oxide-based catalysts was developed, with excellent performance for the selective formation of C_{1-3}-alcohols from syngas. Under reaction condition of 8.0 MPa and 558 K, the space-time-yield of C_{1-3}-alcohols plus dimethyl ether reached 555 mg h^{-1} g^{-1} over the $Ni_1Mo_1K_{0.05}$–11% (5% Ni/CNT) catalyst. The addition of a minor amount of the Ni-decorated CNTs into the $Ni_iMo_jK_k$ host catalyst caused little change in the apparent activation energy for the higher alcohol synthesis (HAS), but led to the increase of the molar percentage of NiO(OH) and Mo^{4+}/Mo^{5+} (the two kinds of catalytically active surface-species related closely to selective formation of C_{1-3}-alcohols) and the dramatic decrease of the molar percentage of Ni^0 and Mo^0 (the two kinds of catalytically active surface-species related closely to selective formation of hydrocarbons, especially methanation of CO). An excellent adsorption performance of the Ni-decorated CNTs for H_2 would be conducive to generating a surface micro-environment with a high concentration of H-adspecies in the form of sp^2-C–H on the functioning catalyst. In addition, high concentration of H-adspecies on the catalyst would greatly inhibit the water-gas-shift side-reaction. All these factors contribute to an increase in the yield of C_{1-3}-alcohols.

1. Introduction

The higher alcohols (C_{2+}-alcohols), together with methanol and dimethyl ether (DME), have been considered as the most important species among coal-based clean synthetic fuels and chemical feedstocks. The higher alcohols have been confirmed to be a better and cleaner automobile fuel. They feature high octane numbers, and lower emissions of NO_x, ozone, CO, and aromatic vapors [1]. Recently, use of methyl *tert*-butyl ether (MTBE) has been prohibited in some countries or regions as additive of oil-based fuel due to the new regulations in environment protection. This change has greatly renewed interest in conversion of syngas via hydrogenation to C_{2+}-oxygenates as gasoline blends [2]. Higher alcohol synthesis (HAS) on the catalysts containing Mo, Group VIII metals and alkali have been extensively studied since the 1980s [3–10]. Progress in this field has contributed considerably to the growing understanding of the nature of those catalytic reaction systems. Nevertheless, the existing technology of HAS is still on a small scale. The single-pass-conversion of the feed-syngas and selectivity to C_{2+}-alcohols are both relatively low. Most systems produce methanol (over alkali-promoted MoS_2 catalysts) or hydrocarbons (over modified Fischer-Tropsch catalysts) as the main product instead of C_{2+}-alcohols [11–13]. Development of catalysts with high efficiency and selectivity for HAS has been one of the key objectives for R&D efforts.

Multi-walled carbon nanotubes (symbolized as "MWCNTs" and simplified as "CNTs" in later text, unless otherwise specified), as a type of novel nano-carbon support or promoter of catalyst, have been drawing increasing attention [14–17] since their discovery [18]. This kind of nanotube-C possesses several unique features, such as highly graphitized tube-wall, nanosized channel and sp^2-C-constructed surface. They also display exceptionally high mechanical strength, high thermal/electrical conductivity, medium to high specific surface areas, and excellent performance for adsorption and spillover of hydrogen, which render this kind of nanostructured carbon materials full of promise as a novel support or promoter of catalyst [14–17]. The catalytic studies conducted so far on CNT-based systems have shown encouraging results in terms of activity and selectivity [19–33].

In the present work, a type of Ni-decorated CNT-promoted co-precipitated Ni–Mo–K oxide-based catalysts was developed with a type of Ni-decorated CNTs as promoter. The catalysts displayed higher catalytic activity and selectivity for HAS from syngas, as

* Corresponding author at: Department of Chemistry, College of Chemistry and Chemical Engineering, Xiamen University, Xiamen 361005, China.
Tel.: +86 592 2184591; fax: +86 592 2086116.
E-mail addresses: chma@xmu.edu.cn (C.-H. Ma), hyli@xmu.edu.cn (H.-Y. Li), gdlin@xmu.edu.cn (G.-D. Lin), hbzhang@xmu.edu.cn (H.-B. Zhang).

0926-3373/$ – see front matter © 2010 Published by Elsevier B.V.
doi:10.1016/j.apcatb.2010.07.040

compared with the CNT-free host catalyst. The catalysts were characterized by means of SEM/TEM/EDS, XRD, XPS, LRS and H_2-TPD, and the nature of promoter action by the CNTs was discussed. The results shed some light on understanding the mechanism of promoter action by the CNT-additive and on the design of practical catalysts for the HAS.

2. Experimental

2.1. Preparation of CNTs and Ni-decorated CNTs

The CNTs used in the present work were "Herringbone-type" CNTs (noted as "CNTs(*h-type*)" and simplified as "CNTs" in later text, unless otherwise specified), which were prepared from catalytic decomposition of CH_4 following the method reported previously [34]. The freshly prepared CNTs were purified by treatment of boiling nitric acid (~8 mol/L) for 12 h, followed by rinsing with the deionized water twice, and then drying at 383 K.

Referring to the method reported by Kurihara et al. [35], Ni-decorated CNTs (symbolized as *x*% Ni/CNTs, where *x*% represents mass percentage of Ni in the *x*% Ni/CNTs) were prepared in the following procedure. About 1 g of $Ni(Ac)_2{\cdot}4H_2O$ (of AR grade) was put into a 100 mL beaker containing 50 mL of 0.050–0.055 M solution of KOH–ethylene glycol, followed by agitating till the Ni precursor salt was completely dissolved and adjusting the pH value of the solution to be 9–10. Approximately 1 g of the purified CNTs were added into the above solution, followed by ultrasonicating for 30 min, microwave-heating for 140 s in a microwave oven (2450 MHz, 800 W), and then rapid-cooling in cold water-bath. The solids were filtered, washed successively with acetone and deionized water, and then dried at 383 K (6 h). The Ni-decorated CNT-material was thus obtained. Element analysis showed that the nickel content was 4.8% (mass percentage) in the prepared material. By changing the loading-amounts of CNTs and $Ni(Ac)_2$, we could prepare a series of *x*% Ni/CNTs with varying Ni contents.

2.2. Preparation of promoted Ni–Mo–K catalysts

A series of (*x*% Ni/CNTs)-promoted Ni–Mo–K oxide-based catalysts, denoted as $Ni_iMo_jK_k$–*y*%(*x*% Ni/CNTs) (where *y*% represented mass percentage), were prepared by using $Ni(NO_3)_2{\cdot}6H_2O$, $(NH_4)_6Mo_7O_{24}{\cdot}4H_2O$, K_2CO_3 (all of AR grade) and the *x*% Ni/CNTs as starting materials following a combined coprecipitation-impregnation method. Two aqueous solutions containing calculated amounts of $Ni(NO_3)_2{\cdot}6H_2O$ and $(NH_4)_6Mo_7O_{24}{\cdot}4H_2O$, respectively, were simultaneously added dropwise under vigorous stirring into a Pyrex flask containing a calculated amount of *x*% Ni/CNTs at constant temperature of 353 K. An appropriate amount of ammonia liquor was added into the aforementioned solution to adjust and maintain the pH value of the solution at ~5 so as to form precipitate. After precipitation, the suspension was continuously stirred for 4 h at 353 K, followed by cooling down to room temperature, aging for 8 h, and filtering. The solids were repeatedly washed with deionized water until the filtrate became neutral in pH, then dried at 383 K (5 h) and further calcined in N_2 atmosphere at 848 K (5 h), followed by cooling down to room temperature. They were next impregnated with K_2CO_3 aqueous solution containing a calculated amount of K by the conventional incipient wetness method, and then dried at 383 K (5 h) and further calcined in N_2 atmosphere at 698 K (4 h), thus yielding the oxide precursor of (*x*% Ni/CNTs)-promoted Ni–Mo–K catalysts. The four reference systems, i.e., the CNT-free host catalyst and the counterparts doped with the simple CNTs(*h-type*) or "parallel-type" CNTs (noted as "CNTs(*p-type*)") [34] or activated carbon (AC), were prepared in the similar way. All samples of catalyst precursor were pressed, crushed, and sieved to a size of 40–80 mesh for the activity evaluation.

2.3. Evaluation of catalyst

Evaluation of the catalyst performance for HAS from syngas was carried out in a fixed-bed continuous-flow reactor and gas chromatograph (GC) combination system. 0.5 g of catalyst sample was used for each test. Prior to the reaction, the sample of catalyst precursor was pre-reduced *in stiu* under purified H_2 stream (0.1 MPa and 1800 mL h^{-1}). The reduction temperature was programmed to rise from room temperature to 623 K and maintain for 12 h, and then decrease to the desired temperature for the catalyst test. The HAS reaction was conducted at a stationary state under reaction conditions of 488–568 K, 2.0–8.0 MPa, $V(H_2)/V(CO)/V(N_2) = 45/45/10$. Exit gas from the reactor was immediately brought down to atmospheric pressure and transported, while its temperature was maintained at 403 K, to the sampling valve of the GC (Model GC-2010 by Shimadzu), which was equipped with dual detectors (TCD and FID) and dual columns filled with carbon molecular sieve (TDX-01) and Porapak Q-S (USA), respectively, for online analysis. The former column (0.8-m length) was used for the analysis of N_2 (as internal standard), CO and CO_2, and the latter (2.0-m length) for C_{1-4}-alkanes, C_{1-4}-alcohols and other oxygenates (mainly DME and acetaldehyde in a small amount). Conversion of CO (X_{CO}) was determined through the internal standard (N_2), and the carbon-based selectivity for the carbon-containing products, including alcohols, hydrocarbons (HC), and other oxygenates (noted as $S_{alc.}$, S_{HC}, etc.), was calculated by an internal normalization method.

2.4. Characterization of catalyst

Transmission electron microscopy (TEM) and scanning electron microscopy (SEM), as well as energy-dispersive X-ray spectroscopy (EDX) were performed with Technai F30 and LEO-1530 electron microscopes, respectively. XRD measurements were carried out on an X'Pert PRO X-ray Diffractometer (PANalytical) with Cu Kα ($\lambda = 0.15406$ nm) radiation. A continuous scan mode was used to collect 2θ data from 10° to 90°. The voltage and current were 40 kV and 30 mA, respectively. X-ray photoelectron spectroscopy (XPS) measurements were done on a Quantum 2000 Scanning ESCA Microprobe instrument with Al Kα radiation (15 kV, 25 W, $h\nu = 1486.6$ eV) under ultrahigh vacuum (10^{-7} Pa), calibrated internally by the carbon deposit C(1*s*) ($E_b = 284.6$ eV). Specific surface area (SSA) was determined by N_2 adsorption using a Micromeritics Tristar-3000 (Carlo Erba) system.

A Renishaw inVia Raman Microscope (equipped with Leica DMLM microscope) was used for Ramen spectral measurements. The 532 nm line from an Ar^+ laser (Renishaw inVia Reflex) was used as the excitation, with an intensity of 4.2 mW. The slit width settings correspond to a resolution of 4 cm^{-1}. A home-made high-temperature sample cell was used in this study. The reduction of catalyst samples and the chemisorption experiments, as well as Raman spectral recordings, were conducted *in situ*. Spectral accumulation was necessary; up to 120 scans were accumulated in some cases to obtain a decent signal-to-noise ratio.

Tests of H_2-temperature-programmed desorption (TPD) of catalyst were conducted on an adsorption/desorption system. 200 mg of sample of the catalyst precursor was used in each test. Prior to the TPD test, the sample of catalyst was *in situ* pre-reduced in a H_2 (of 99.999% purity) stream at 623 K (6 h) and then flushed by an Ar (of 99.999% purity) stream at 623 K (1 h) to clean its surface, followed by cooling down to 433 K, switching to the H_2 stream for hydrogen adsorption at 433 K (60 min) and subsequently at room temperature (120 min). After that, the sample was flushed by the Ar

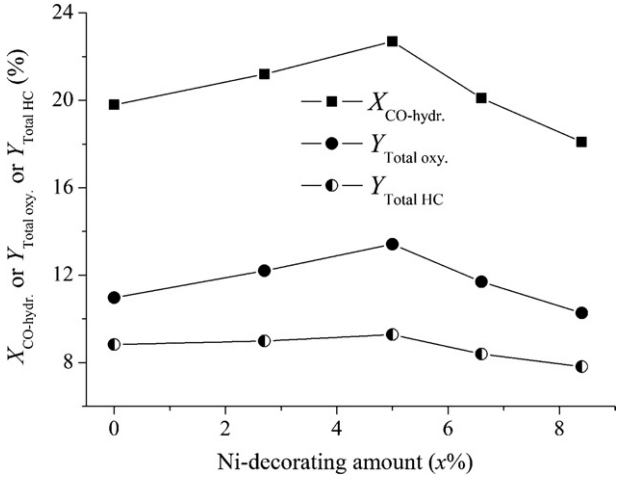

Fig. 1. HAS reactivity over the $Ni_1Mo_1K_{0.05}$–11% (*x*% Ni/CNTs) catalysts with varying Ni-decorating amounts at: 2.0 MPa, 543 K, $V(H_2)/V(CO)/V(N_2) = 60/30/10$, GHSV = 3000 $mL_{STP}\ h^{-1}\ g^{-1}$ (outlet).

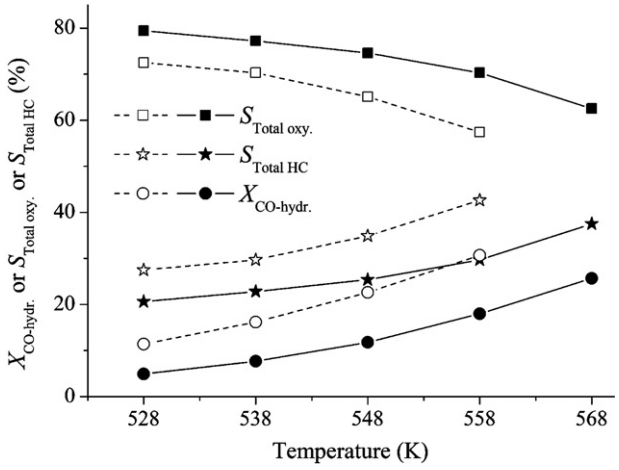

Fig. 2. HAS reactivity over the $Ni_1Mo_1K_{0.05}$–11% (5% Ni/CNTs) catalyst with varying temperatures. Reaction conditions: 5.0 MPa, $V(H_2)/V(CO)/V(N_2) = 60/30/10$ (hollow mark) or 45/45/10 (solid mark), GHSV = 5000 $mL_{STP}\ h^{-1}\ g^{-1}$ (outlet).

stream at room temperature till the stable baseline of GC appeared, followed by starting to conduct the TPD measurement from 298 K to 873 K. The rate of temperature increase was 5 K min^{-1}. The desorbed exit-gases were analyzed by an on-line GC (Shimadzu GC-8A) with a thermal conductivity detector (TCD).

3. Results and discussion

3.1. HAS reactivity over the CNT-containing (or free) Ni–Mo–K catalysts

We first investigated the reaction activity of HAS from syngas over a series of the simple CNT-promoted catalysts, $Ni_iMo_jK_k$–*y*% CNTs, with varied CNT-additive levels, Ni/Mo and K/Mo molar ratios. The results indicated that the catalyst with the composition of $Ni_1Mo_1K_{0.05}$–11% CNTs displayed the highest catalytic activity for the HAS from syngas.

Next, with $Ni_1Mo_1K_{0.05}$ as host and using the Ni-decorated CNTs in place of the simple CNTs as the promoter while maintaining the same additive level (11%), the promoting effect of decoration of metallic Ni to CNTs on the performance of the corresponding catalyst for the HAS was investigated. The results indicated that the observed carbon-containing products included C_{1-3}-alcohols and DME (noted as "C_{1-3}-oxygenates" or "total oxygenates") and C_{1-4}-hydrocarbons (noted as "total HC"), as well as CO_2 (yielded from WGS side-reaction), and that the $Ni_1Mo_1K_{0.05}$–11% (5% Ni/CNTs) catalyst displayed the best catalytic performance (see Fig. 1). Under the reaction conditions of 2.0 MPa, 543 K, $V(H_2)/V(CO)/V(N_2) = 60/30/10$ and GHSV = 3000 $mL_{STP}\ h^{-1}\ g^{-1}$, the conversion of CO hydrogenation (noted as $X_{CO\text{-}hydr.}$) reached 22.7%, with the corresponding total oxygenate yield (i.e., the product of $X_{CO\text{-}hydr.}$ and $S_{Total\ oxy.}$, symbolized as $Y_{Total\ oxy.}$) reaching 13.4% over this catalyst. Over the other four catalysts promoted by the *x*% Ni/CNTs (*x*% = 0%, 2.7%, 6.6% and 8.4%, respectively), the $X_{CO\text{-}hydr.}$ was 19.8%, 21.2%, 20.1%, 18.1%, successively, with the corresponding $Y_{Total\ oxy.}$ values being 11.0%, 12.2%, 11.7%, 10.3%, respectively.

Fig. 2 showed the reactivity of HAS over the $Ni_1Mo_1K_{0.05}$–11% (5% Ni/CNTs) catalyst with varying temperatures. With increasing reaction temperature, $X_{CO\text{-}hydro.}$ increased monotonously, with the descent of $S_{Total\ oxy.}$ being slow at temperatures below 558 K, but accelerated when the temperatures went up to 558 K. In order to obtain high yield of alcohols and low consumption of feed-gas, 558 K was taken as the optimal operating temperature.

The experiments also revealed that an appropriately low H_2/CO molar ratio in the feed-syngas is favorable to the formation of C_{1-3}-oxygenated products. When fed with the feed-syngas of $H_2/CO = 1$ (molar ratio) (i.e., $V(H_2)/V(CO)/V(N_2) = 45/45/10$), the $X_{CO\text{-}hydr.}$ and $S_{Total\ oxy.}$ reached 18.0% and 70.3%, respectively, at the optimal reaction temperature (558 K), with the corresponding space-time-yield of total oxygenates ($STY_{Total\text{-}oxy.}$) reaching 379 mg $h^{-1}\ g^{-1}$. In comparison, these values were 30.7% (for $X_{CO\text{-}hydr.}$), 57.4% (for $S_{Total\ oxy.}$) and 358 mg $h^{-1}\ g^{-1}$ (for $STY_{Total\text{-}oxy.}$) under the reaction conditions of 5.0 MPa, 558 K, $V(H_2)/V(CO)/V(N_2) = 60/30/10$ and GHSV = 5000 $mL_{STP}\ h^{-1}\ g^{-1}$. Therefore, a high H_2/CO molar ratio improves CO hydrogenation-conversion at the cost of selectivity for total oxygenates, and does not increase the space-time-yield of total oxygenates.

Fig. 3 showed the product distribution of HAS over the CNT-containing catalysts and the CNT-free host system under the reaction conditions of 5.0 MPa, 558 K, $V(H_2)/V(CO)/V(N_2) = 45/45/10$, GHSV = 5000 $mL_{STP}\ h^{-1}\ g^{-1}$. The products of CO hydrogenation were the mixtures consisting of linear primary alcohols, hydrocarbons and DME, but the carbon-number distribution of the alcohols and hydrocarbons did not follow a classical Anderson-Schulz-Flory rule well.

It can be seen from the results shown in Fig. 3 and Table 1 that addition of an appropriate amount of the CNTs, especially the Ni-decorated CNTs, into the $Ni_1Mo_1K_{0.05}$ host catalyst improved dramatically the selectivity for formation of higher alcohols, with the $S_{Total\ oxy.}$ from 33.2% for the CNT-free host catalyst ($Ni_1Mo_1K_{0.05}$) going up to 70.3% for the $Ni_1Mo_1K_{0.05}$–11% (5% Ni/CNTs) catalyst under the reaction conditions of 5.0 MPa, 558 K, $V(H_2)/V(CO)/V(N_2) = 45/45/10$ and GHSV = 5000 $mL_{STP}\ h^{-1}\ g^{-1}$. This led to a considerable increase in $STY_{Total\ oxy.}$, i.e., from 218 mg $h^{-1}\ g^{-1}$ for the former going up to 379 mg $h^{-1}\ g^{-1}$ for the latter (increased by 74%). Moreover, the WGS side-reaction was greatly inhibited, with the CO conversion via WGS from 18.6% for the former coming down to 5.1% for the latter under the same reaction conditions. EtOH was the dominant product of CO hydrogenation, with the carbon-based selectivity reaching 24.3%, while correspondingly the selectivity of MeOH, PrOH and DME being 18.7%, 10.4%, and 16.9%, respectively.

Fig. 4 showed the stability of the $Ni_1Mo_1K_{0.05}$–11% (5% Ni/CNTs) catalyst for HAS continuing up to 200 h under the two types of reaction conditions with varying pressures and GHSVs. After about 24 h of "running in" stage of the reaction, the catalyst attained a stable operating state, with no obvious deactivation observed after

Table 1
Reactivity of HAS over the Ni-decorated CNT-promoted Ni–Mo–K catalyst and the related reference systems (prepared in the similar way).

Catalyst	React. conditions	Conversion of CO (%)		Selectivity of hydrogenation product (C%)						$STY_{Total\ oxy.}$ ($mg\,h^{-1}\,g^{-1}$)
		Hydrogenation	WGS	Total oxy.	HCs	MeOH	EtOH	PrOH	DME	
$Ni_1Mo_1K_{0.05}$–11% (5% Ni/CNTs(*h-type*))	(a)	18.0	5.1	70.3	29.7	18.7	24.3	10.4	16.9	379
	(b)	13.8	1.6	70.2	29.8	18.6	24.4	9.8	17.4	555
$Ni_1Mo_1K_{0.05}$–11% CNTs (*h-type*)	(a)	15.5	4.1	69.8	30.2	19.6	23.4	10.1	16.7	317
$Ni_1Mo_1K_{0.05}$–11% AC	(a)	17.4	16.4	33.8	66.2	18.9	5.9	2.8	6.2	194
$Ni_1Mo_1K_{0.05}$–11% CNTs (*p-type*)	(a)	15.3	11.1	45.1	54.9	19.7	10.1	4.0	11.3	212
$Ni_1Mo_1K_{0.05}$	(a)	19.4	18.6	33.2	66.8	18.3	6.5	2.1	6.3	218
5% Ni/CNTs (*h-type*)	(a)	9.6	0	53.7	46.3 (34% for CH_4)	25.8	14.3	7.4	6.2	153

Reaction conditions: (a) 5.0 MPa, 558 K, $V(H_2)/V(CO)/V(N_2) = 45/45/10$, GHSV = 5000 $mL_{STP}\,h^{-1}\,g^{-1}$; (b) 8.0 MPa, 558 K, $V(H_2)/V(CO)/V(N_2) = 45/45/10$, GHSV = 10,000 $mL_{STP}\,h^{-1}\,g^{-1}$.

the reaction for 200 h. Under the reaction conditions of 8.0 MPa, 558 K, $V(H_2)/V(CO)/V(N_2) = 45/45/10$, GHSV = 10000 $mL_{STP}\,h^{-1}\,g^{-1}$, the $X_{CO\text{-}hydr.}$ reached 13.8%, with the corresponding $S_{Total\ oxy.}$ and $STY_{Total\ oxy.}$ reaching 70.2% and 555 $mg\,h^{-1}\,g^{-1}$, respectively (see Table 1). The combined mass% of C_{2-3}-alcohols and DME reached 66% in the total oxygenated products, showing great potential in commercial use for the HAS.

It can be seen from Table 1 that CNTs(*p-type*)-doped counterpart displayed the rather limited promoter effect for selective formation of the oxygenate products, while the addition of AC, a kind of amorphous carbon with 830 m^2/g of N_2-BET-SSA, into the $Ni_1Mo_1K_{0.05}$ host catalyst not only did not help increase selectivity of the oxygenate products, but also led to a certain decrease of the $X_{CO\text{-}hydr.}$ and $STY_{Total\ oxy.}$.

Table 1 also lists the result of "blank" catalytic measurement with 5% Ni/CNTs, showing that the Ni-decorated CNTs displayed fairly high activity for hydrogenation-conversion of CO under the reaction conditions for the HAS, with methane ($S_{CH4} \approx 34.0\%$) and methanol ($S_{MeOH} \approx 25.8\%$) as the dominant products. Such results are consistent with the well-known fact that metallic Ni is a good catalyst for hydrogenation (especially methanation) of CO. Yet in the present work when used as additive, metal Ni has little direct contribution to the hydrogenation-conversion of syngas, most probably due to its low content and to being covered with the Ni–Mo host components.

The apparent activation energy (E_a) of the HAS reaction was measured under the reaction conditions with mass transfer limitation ruled out, and the results are shown in Fig. 5. Over the three catalysts of $Ni_1Mo_1K_{0.05}$–11% (5% Ni/CNTs), $Ni_1Mo_1K_{0.05}$–11% CNTs and $Ni_1Mo_1K_{0.05}$, the observed E_a of the HAS reaction was 90.6, 93.0 and 88.0 $kJ\,mol^{-1}$, respectively, under the reaction conditions of 2.0 MPa, 523–563 K, $V(H_2)/V(CO)/V(N_2) = 60/30/10$, GHSV = 12000 $mL_{STP}\,h^{-1}\,g^{-1}$. These E_a values were fairly close to each other, indicating that addition of an appropriate amount of either the simple CNTs or the Ni-decorated CNTs into the $Ni_1Mo_1K_{0.05}$ host catalyst did not cause a marked change in the E_a for the HAS reaction, implying that the addition of a minor amount of either the simple CNTs or the Ni-decorated CNTs to the $Ni_1Mo_1K_{0.05}$ did not alter the reaction pathway of rate-determining step of the CO hydrogenation reaction.

3.2. SEM/TEM and EDX characterizations of Ni-decorated CNTs

It is quite evident that the high reactivity (esp. high selectivity of formation of C_{1-3}-oxygenates) of HAS over the Ni–Mo–K catalyst doped by the CNTs (or *x*% Ni/CNTs) is closely related to the unique properties of the CNTs (or *x*% Ni/CNTs) as promoter. The CNTs used in the present work were a "Herringbone-type" of multi-walled carbon nanotubes [34,36]. Previous characterization studies demonstrated that the outer diameters of those CNTs were in the range of 15–50 nm, the inner diameters in 3–7 nm and the N_2-BET surface area at approximately 130 $m^2\,g^{-1}$. The contents of elemental carbon and graphitized carbon were ≥99.5% and >90% (mass percentage), respectively, in the purified CNTs. Test of H_2-temperature-programmed hydrogenation (TPH) showed that the temperature needed for initiating the hydrogenation reaction of the CNTs with H_2 was ≥773 K [37], indicating that this type of CNTs was stable in H_2-atmosphere at the reaction temperatures for the HAS.

Fig. 6 showed the SEM/TEM images and EDX spectrum of the 5% Ni/CNTs. It can be seen from Fig. 6(a) and (b) that the Ni nanoparticles dispersed well and scattered on the outer and inner surface of the CNTs. The Ni-particle diameters were estimated to be below 2 nm. The EDX analysis (Fig. 6(c)) further demonstrated that carbon, oxygen and nickel were the only three elements at the surface of 5% Ni/CNTs, with atomic percentage of 94.4%, 4.5% and 1.1%, respectively. The corresponding mass percentages were 89.3%, 5.6% and 5.1%, respectively. The surface oxygen originated most probably from the preoxidation and carboxylation treatment of the CNTs by the concentrated nitric acid.

3.3. Post-analysis of the tested catalysts by XRD and XPS

The XRD post-analysis of the catalysts tested for HAS under the aforementioned reaction conditions showed that there was significant difference between the CNT-containing catalysts and the CNT-free host system in the position and shape of their XRD features (Fig. 7). On the two CNT-containing catalysts, the observed XRD features at $2\theta = 26.1^\circ$, 43.1° and 53.5° were due to the diffraction of (0 0 2), (1 0 0) and (0 0 4) faces of graphitized carbon of the CNTs, respectively [36,38]. Their Ni and Mo components existed mainly in the form of $Ni_2Mo_3O_8$ ($2\theta = 17.9^\circ$, 19.9°, 25.4°, 32.6°, etc.) and secondly in NiO ($2\theta = 43.3^\circ$) and MoO_2 ($2\theta = 26.3^\circ$, 37.0°, 49.8°, 53.8°) [39], although the presence of alloy phases of $Mo_{0.84}Ni_{0.16}$ and $MoNi_4$ (with the weak, even ambiguous, XRD features at $2\theta = 61.3^\circ$ and 74.7°, respectively) could not be excluded. On the CNT-free host catalyst, the observed crystallite phases ascribed to the Ni and Mo components were mainly $Mo_{0.84}Ni_{0.16}$ ($2\theta = 36.8^\circ$, 42.6°, 61.3°) and $MoNi_4$ ($2\theta = 44.1^\circ$, 50.4°, 74.7°) alloys [39].

The XPS post-analysis of the tested catalysts revealed that significant difference between the CNT-containing catalysts and the CNT-free host system also existed in the valence-state or micro-environment of their surface Ni and Mo species. Referring to Ref. [40] and through computer-fitting, we found that each of the Ni(2*p*)-XPS spectra (Fig. 8(A)) contained the contribution from four kinds of surface Ni-species with different valence-states or micro-environments. At the quasi-functioning surface of the two CNT-containing catalysts, the major Ni-species was NiO(OH) [Ni($2p_{3/2}$) = 856.3 eV (B.E.)], secondary was $Ni(OH)_2$ [Ni($2p_{3/2}$) = 855.7 eV (B.E.)] and NiO [Ni($2p_{3/2}$) = 853.3 eV (B.E.)], while Ni^0 [Ni($2p_{3/2}$) = 852.7 eV (B.E.)] was in minority. In contrast to the cases of the CNTs (or 5% Ni/CNTs)-doped systems, at the

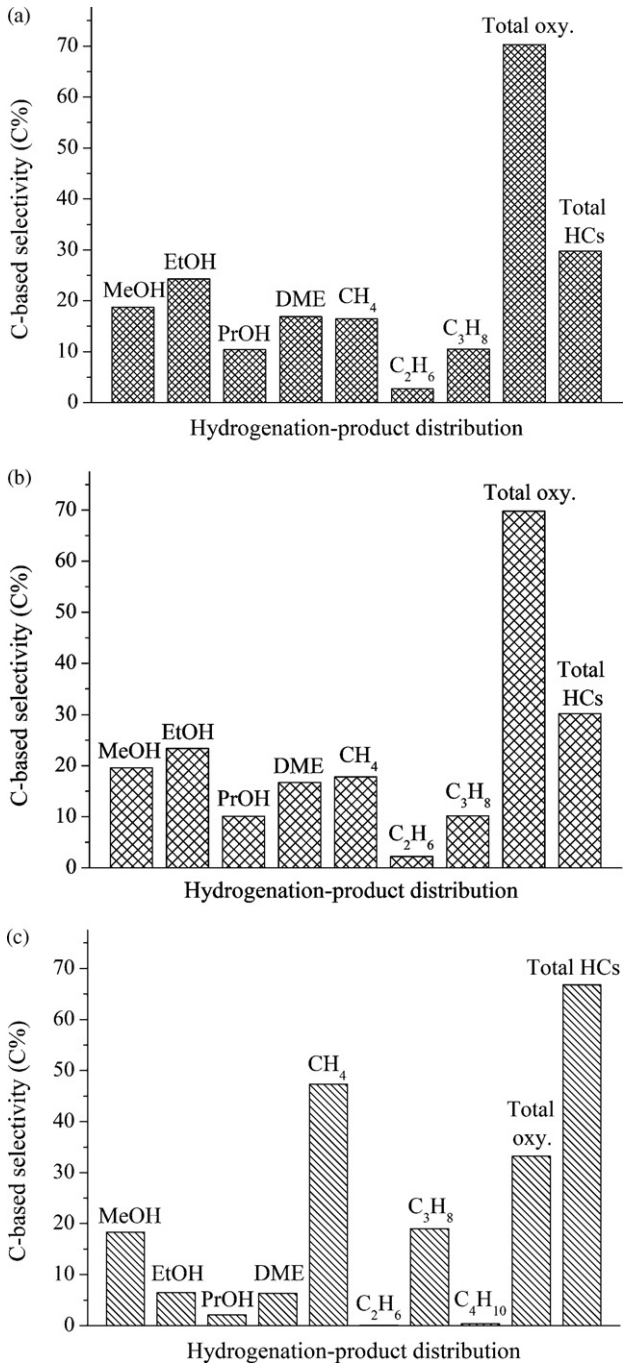

Fig. 3. Product distribution of HAS over the catalysts: (a) $Ni_1Mo_1K_{0.05}$–11% (5% Ni/CNTs); (b) $Ni_1Mo_1K_{0.05}$–11% CNTs; (c) $Ni_1Mo_1K_{0.05}$; reaction conditions: 5.0 MPa, 558 K, $V(H_2)/V(CO)/V(N_2) = 45/45/10$, GHSV = 5000 $mL_{STP}\ h^{-1}\ g^{-1}$ (outlet).

quasi-functioning surface of the CNT-free host catalyst, the major Ni-species was Ni^0, secondary NiO(OH) and $Ni(OH)_2$, while NiO in minority (see Table 2).

Analysis and fitting of the Mo(3*d*)-XPS spectra (Fig. 8(B)) were also done following Ref. [41]. The results showed that, at the quasi-functioning surface of the CNTs (or 5% Ni/CNTs)-doped catalysts, most of the Mo^{6+} [$Mo(3d_{5/2}) = 232.6$ eV (B.E.)] was reduced to lower valence: major portion to Mo^{5+} [$Mo(3d_{5/2}) = 230.9$ eV (B.E.)] and minor to Mo^{4+} [$Mo(3d_{5/2}) = 229.8$ eV (B.E.)]. This was analogous to the case of co-existence of Mo^{4+} with Mo^{5+} (major) and Mo^{6+} (minor) in the related systems [42]. However at the quasi-functioning surface of the CNT-free host, about a half of the Mo^{6+}

Table 2
XPS binding energy and relative content (mol%) of the Ni and Mo species with different valence-states or micro-environments at the surface of the HAS-tested catalysts.

Catalyst sample	Relative content (mol%)							
	Ni^0 with $Ni(2p_{3/2}) \approx 852.7$ eV (B.E.)	NiO with $Ni(2p_{3/2}) \approx 853.3$ eV (B.E.)	$Ni(OH)_2$ with $Ni(2p_{3/2}) \approx 855.7$ eV (B.E.)	NiO(OH) with $Ni(2p_{3/2}) \approx 856.3$ eV (B.E.)	Mo^0 with $Mo(3d_{5/2}) \approx 228.6$ eV (B.E.)	Mo^{4+} with $Mo(3d_{5/2}) \approx 229.8$ eV (B.E.)	Mo^{5+} with $Mo(3d_{5/2}) \approx 230.9$ eV (B.E.)	Mo^{6+} with $Mo(3d_{5/2}) \approx 232.6$ eV (B.E.)
$Ni_1Mo_1K_{0.05}$–11% (5% Ni/CNTs)	2.6	13.2	18.4	65.8	–	12.3	54.8	32.9
$Ni_1Mo_1K_{0.05}$–11% CNTs	4.4	12.9	18.0	64.7	–	9.1	51.9	39.0
$Ni_1Mo_1K_{0.05}$	54.6	4.0	16.6	24.8	46.2 NiMo-alloy	4.9	5.3	43.6

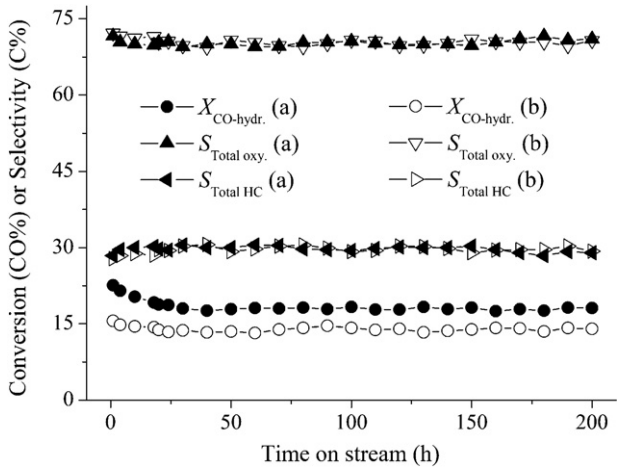

Fig. 4. Operation stability of HAS lasting 200 h over $Ni_1Mo_1K_{0.05}$–11% (5% Ni/CNTs) catalyst; reaction conditions: (a) the same as in Fig. 3; (b) 8.0 MPa, 558 K, $V(H_2)/V(CO)/V(N_2) = 45/45/10$ and GHSV = 10,000 $mL_{STP}\ h^{-1}\ g^{-1}$ (outlet).

was reduced to Mo^0, most probably in the form of Ni–Mo alloys [Mo($3d_{5/2}$) = 228.6 eV (B.E.)], and the content of Mo^{5+} and Mo^{4+} species was extremely low (see Table 2).

The aforementioned XPS results were in good agreement with the XRD results, and strongly implied that it was those surface NiO(OH) and Mo^{4+}/Mo^{5+} species that were closely related to highly selective formation of the C_{1-3}-alcohols.

3.4. LRS characterizations of hydrogen adsorption on pre-reduced catalysts

In situ laser Raman spectroscopy (LRS) was used to investigate the H_2 adsorption on the pre-reduced catalysts. The results provide the useful information about the nature of the hydrogen-adsorption sites and the corresponding H-adspecies at the surface of these catalysts. Fig. 9 are the Ramen spectra in the region of 1750–3350 cm^{-1} of hydrogen species adsorbed on the pre-reduced catalysts after 16 h of reduction by H_2 at 623 K, followed by cooling down to room temperature in a flow of H_2 (of 99.999% purity, flow rate of 3600 mL h^{-1}). On the two CNT-containing catalysts, the observed Raman bands are present at 2331 (w), 2695 (s), 2935 (m), and 3233 (m) cm^{-1} (see Fig. 9(a) and (b)). As has been previously indicated [43], the weak 2331-cm^{-1} peak is due to the stretching mode of free dinitrogen existing in the atmosphere associated with the general sample compartment region of the spectrometer, which can be conveniently used for calibration of the spectrometer. The region at 1750–3350 cm^{-1} of these spectra corresponds closely to our spectra reported for the second-order combination modes of the first-order Raman mode E_{2g} and the defect-induced D mode of graphitized carbon (sp^2-C), which appeared at 1580 and 1346 cm^{-1} when using the 514-nm line from an argon ion laser as excitation [38,44]. Consequently, the bands at 2695 and 2935 cm^{-1} can be ascribed to the second-order combination frequencies, 2D and D + E_{2g}, respectively, of the sp^2-C; while 3233-cm^{-1} band may reasonably be attributed to stretching vibration of (sp^2-C)–H for hydrogen adsorbed on the CNTs.

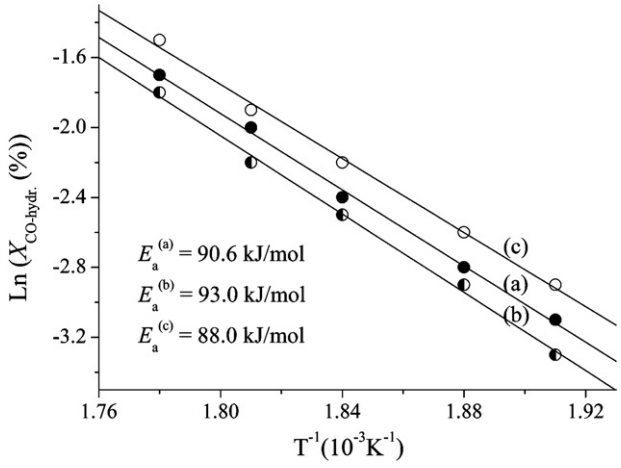

Fig. 5. Arrhenius plots of HAS over the catalysts: (a) $Ni_1Mo_1K_{0.05}$–11% (5% Ni/CNTs); (b) $Ni_1Mo_1K_{0.05}$–11% CNTs; (c) $Ni_1Mo_1K_{0.05}$; taken at 2.0 MPa, 523–563 K, $V(H_2)/V(CO)/V(N_2) = 60/30/10$, GHSV = 12,000 $mL_{STP}\ h^{-1}\ g^{-1}$ (outlet).

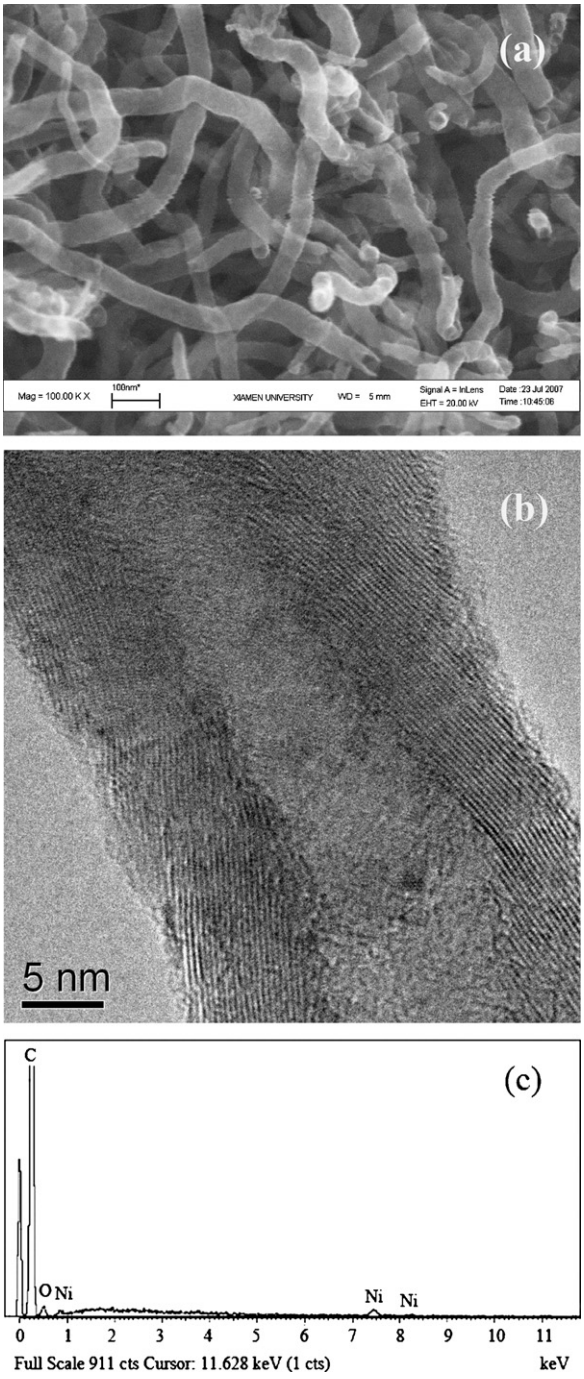

Fig. 6. SEM (a) and TEM (b) images and energy-dispersive X-ray (EDX) spectrum (c) of the 5% Ni/CNTs.

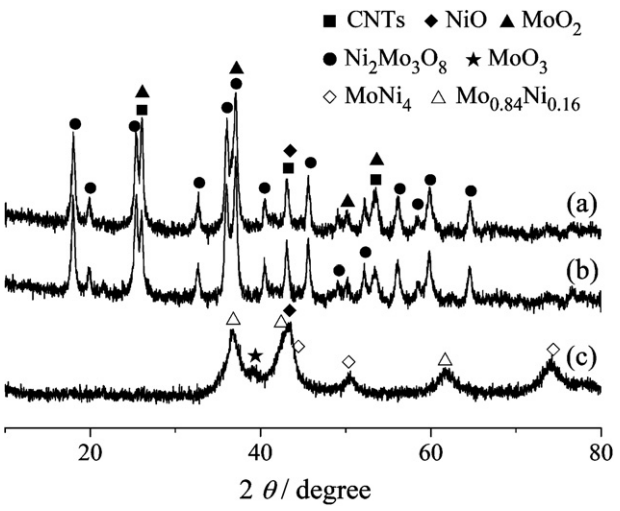

Fig. 7. XRD patterns of the HAS-tested catalysts: (a) $Ni_1Mo_1K_{0.05}$–11% (5% Ni/CNTs); (b) $Ni_1Mo_1K_{0.05}$–11% CNTs; (c) $Ni_1Mo_1K_{0.05}$.

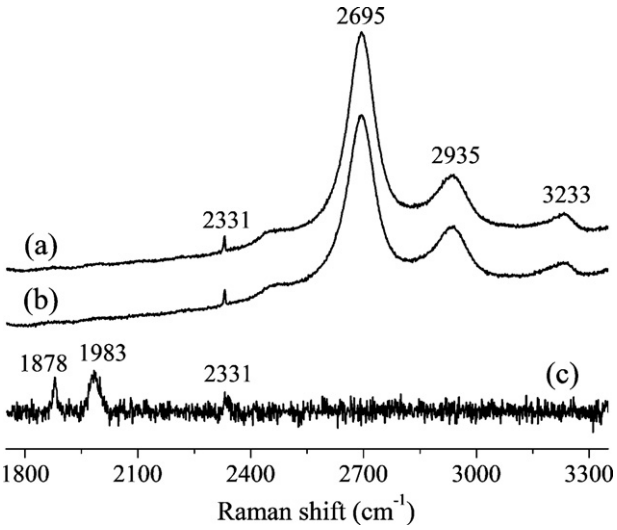

Fig. 9. Raman spectra of hydrogen adsorption on pre-reduced catalysts: (a) $Ni_1Mo_1K_{0.05}$–11% (5% Ni/CNTs); (b) $Ni_1Mo_1K_{0.05}$–11% CNTs; (c) $Ni_1Mo_1K_{0.05}$.

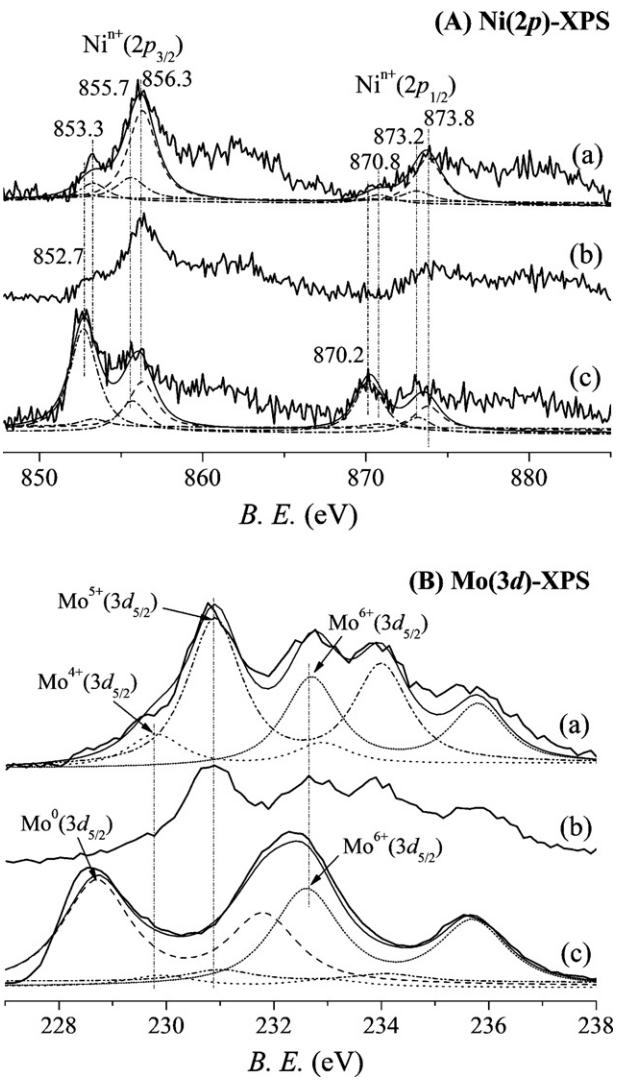

Fig. 8. XPS spectra of Ni(2*p*) (A) and Mo(3*d*) (B) of the HAS-tested catalysts: (a) $Ni_1Mo_1K_{0.05}$–11% (5% Ni/CNTs); (b) $Ni_1Mo_1K_{0.05}$–11% CNTs; (c) $Ni_1Mo_1K_{0.05}$.

In contrast to the cases of the two CNT-containing catalysts, only two Ramen bands at 1878 (m) and 1983 (m) cm^{-1} were observed on the CNT-free host system. According to Kaesz and Saillant [45], and Johnson and Lewis [46], the M–H streching frequency for terminally bonded hydrogen in most transition-metal molecular clusters falls in the range of 1850–2200 cm^{-1}. Kavtaradze and Sokolova [47] have reported that the adsorption of hydrogen on alumina-supported iron, cobalt, and nickel is dissociative. The infrared or Raman bands of the corresponding surface hydrides are in the range of 1850–1980 cm^{-1} [47,48]. Consequently, the bands 1878 and 1983 cm^{-1} may be reasonably assigned to stretching vibrations of metal molybdenum–hydrogen (Mo^0–H) and metal nickel–hydrogen (Ni^0–H), respectively.

From the aforementioned results, it can be inferred that, on the pre-reduced CNT-containing catalysts, the surface-sites responsible for adsorption-activation of H_2 were mainly the (sp^2-C)-sites with surface dangling bond, with (sp^2-C)–H being dominant surface H-adspecies; while on the pre-reduced CNT-free host catalyst, the surface-sites responsible for adsorption-activation of H_2 were mainly the zero-valent transition-metal sites (Ni_x^0- and Mo_x^0-sites), with the Ni^0–H and the Mo^0–H being predominant surface H-adspecies.

3.5. H_2-TPD test of hydrogen adsorption on pre-reduced catalysts

The previous studies by Ishikawa et al. [49] demonstrated that graphitized carbon black surfaces were capable of rapidly equilibrating H_2/D_2 mixtures. A dissociation rate of 2.5×10^{17} molecules/(s(m^2-ASA)) was measured at ambient temperatures and pressures. The ASA (active surface area) was described in terms of atoms located at edge positions on the graphite basal plane and was determined from the amount of oxygen able to chemisorb at these sites, regardless of the nature of the carbon material under investigation. The H_2-TPD investigation by Zhou et al. [50] showed that hydrogen adsorption on the CNTs can occur at ambient temperatures and pressures, and that the desorbed product was almost exclusively H_2 at temperatures lower than 773 K, while it included CH_4, C_2H_4 and C_2H_2, in addition to H_2, at temperatures of 773 K and above. This implies that H_2 adsorption on the CNTs may be in two forms: associative (molecular state) and dissociative (atomic state), as had been evidenced in our LRS studies of H_2/CNTs adsorption system [38].

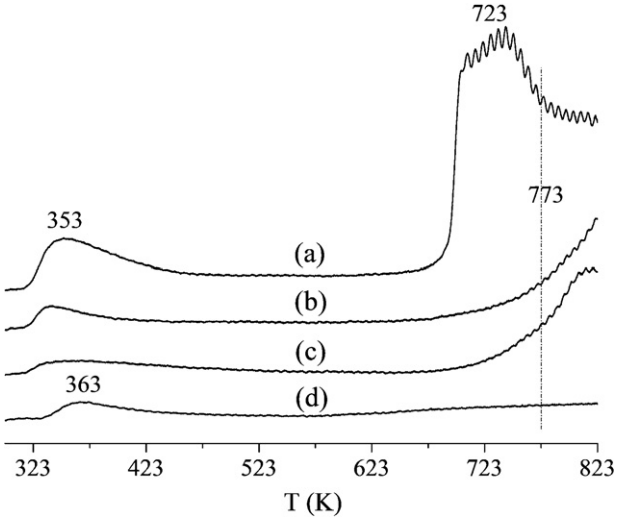

Fig. 10. H_2-TPD profiles of H_2 adsorption on varying carbon-materials: (a) 5% Ni/CNTs(*h-type*); (b) CNTs(*h-type*); (c) CNTs(*p-type*); (d) AC.

Fig. 10 showed the H_2-TPD profiles of hydrogen adsorbed at 433K followed by cooling down to room temperature on varying carbon-materials respectively. The decoration of metallic nickel to the CNTs resulted in a significant increase in their capacity of adsorbing hydrogen, especially dissociatively adsorbing hydrogen (Fig. 10(a) vs. Fig. 10(b)). Considering that the hydrogenation of some surface carbon by H-adspecies (which would lead to consumption of part of H-adspecies and formation of C_{1-2}-hydrocarbons) could occur at temperatures of 773 K and above [50], we estimated the relative area-intensity (I) of these H_2-TPD profiles in the region of 298–773 K. The obtained ratio was: $I_{(a)}/I_{(b)}/I_{(c)}/I_{(d)} = 100/26/19/16$.

Fig. 11 showed the H_2-TPD profiles of hydrogen adsorbed on the pre-reduced catalysts. The two H_2-TPD profiles taken on the two CNT-containing systems were similar to each other in the position and shape as well as relative intensity of their H_2-TPD features (see Fig. 11(a) and (b)). The aforementioned result of LRS characterization has shown that most H-adspecies at the surface of the hydrogen-pre-reduced CNTs(or 5% Ni/CNTs)-doped Ni–Mo–K catalyst were in the form of (sp^2-C)–H. Consequently, the 373-K peak (spanning from 298 K to 548 K) was due to desorption of H-species

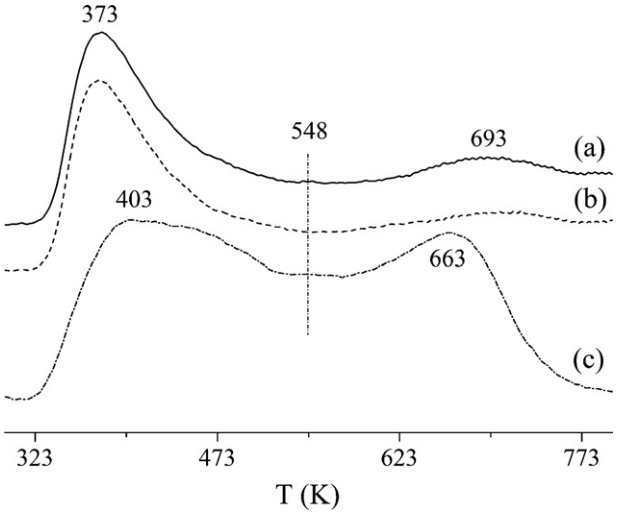

Fig. 11. H_2-TPD profiles of hydrogen adsorption on pre-reduced catalysts: (a) $Ni_1Mo_1K_{0.05}$–11% (5% Ni/CNTs); (b) $Ni_1Mo_1K_{0.05}$–11% CNTs; (c) $Ni_1Mo_1K_{0.05}$.

adsorbed weakly on the CNTs, and the 693-K peak (spanning from 548 K to 773 K) may be ascribed to desorption of H-species chemisorbed strongly (probably dissociatively) on the CNTs. The ratio of the total relative area-intensity of the two H_2-TPD profiles in the range of 298–773 K was estimated to be $I_{(a)}/I_{(b)} = 100/88$. This suggested that the sequence of increasing surface concentration of H-adspecies on the functioning catalysts was: $Ni_1Mo_1K_{0.05}$–11% (5% Ni/CNTs) > $Ni_1Mo_1K_{0.05}$–11% CNTs, in line with the observed sequence of reaction activity of HAS over the two catalysts.

On the CNT-free co-precipitated host system ($Ni_1Mo_1K_{0.05}$), the observed H_2-TPD peaks were present at 403 and 663 K (see Fig. 11(c)). In connection with the results of the aforementioned XRD, XPS and LRS characterizations of this catalyst, it could be inferred that the involved H-adspecies was mainly those adsorbed on the zero-valent transition-metal sites (Ni_x^0- and Mo_y^0-sites) at the catalyst surface. The 403-K peak was due to desorption of weakly adsorbed H-species, while the 663-K peak may be ascribed to the desorption of H-species chemisorbed strongly, most probably dissociatively.

3.6. Nature of promoter action by the CNTs

It is quite evident that the high selectivity to formation of C_{1-3}-alcohols over the CNTs(or 5% Ni/CNTs)-doped catalysts is closely related to the sp^2-C structure and some properties of the CNTs. The aforementioned results indicated that the addition of a minor amount of the CNTs(or 5% Ni/CNTs) to the $Ni_1Mo_1K_{0.05}$ host catalyst did not cause a marked change in the E_a for the reaction of CO hydrogenation to generate C_{1-3}-alcohols, but led to a dramatic increase, at the surface of the functioning catalyst, of the molar percentage of NiO(OH) and Mo^{4+}/Mo^{5+} species active catalytically in the respective total amounts of Ni and Mo, and meanwhile, brought about the significant change of surface H-adspecies in the nature: the concentration of H-adspecies in the form of transition-metal hydrides (Ni^0–H and Mo^0–H) dramatically decreased while simultaneously generating a great number of H-adspeies in the form of (sp^2-C)–H. This resulted in a significant change of the surface properties and micro-environments of the catalyst. The catalytic function for methanation was greatly weakened and the probability of carbon-chain growing and terminating to form C_{1-3}-alcohols remarkably increased, thus significantly improving the selectivity to formation of C_{1-3}-alcohols in the HAS reaction.

Compared to that of the CNTs(*h-type*), the surface of the "Parallel-type" CNTs (symbolized as CNTs(*p-type*)) possesses less dangling bonds, thus lower chemical activity [17,34,36,38]. It is probably this peculiarity that renders the CNTs(*p-type*) to have lower capability for adsorption and activation of H_2 (with the relative area-intensity of the H_2-TPD profile of the latter to be merely 73% of that of the former in the range of 298–773 K, as estimated from Fig. 10(c) vs. Fig. 10(b)), thus showing the rather limited promoter effect (see Table 1).

In sharp contrast to the CNTs (or 5% Ni/CNTs)-doped systems, the addition of AC into the $Ni_1Mo_1K_{0.05}$ host catalyst did not help improve the performance of the catalyst, and further led to a certain decrease in the $X_{CO\text{-}hydr.}$ and $STY_{Total\ oxy.}$ (see Table 1). It appears that the presence of AC simply dilutes the active components of the catalyst.

4. Concluding remarks

(1) The CNTs, especially Ni-decorated CNTs, can serve as a novel promoter of the Ni–Mo–K host catalyst for HAS. The (5% Ni/CNTs)-doped $Ni_1Mo_1K_{0.05}$ catalyst achieves highly effective and selective formation of C_{1-3}-alcohols from syngas.

(2) The promoter action by the CNTs was mainly in providing the sp^2-C surface-sites for adsorption-activation of H_2 (one of the reactants), while simultaneously enhancing the molar percentage of the two kinds of catalytically active species, NiO(OH) and Mo^{4+}/Mo^{5+} (both related closely to selective formation of C_{1-3}-alc.), via affecting the chemical states of catalyst.
(3) Appropriate decoration of the CNTs by a minor amount of metallic nickel could improve the capability of CNT's adsorbing H_2, rendering their promoter action more remarkable.

Acknowledgements

The work is supported by National Basic Research ("973") Project (2009CB939804) and Fujian Provincial Key Scientific & Technical Projects (2009HZ0002-1 and 2009HT1030) of China.

References

[1] R.R. Chianelli, J.E. Lyons, G.A. Mills, Catal. Today 22 (1994) 361–396.
[2] N.D. Subramanian, G. Balaji, C.S.S.R. Kumar, J.J. Spivey, Catal. Today 147 (2) (2009) 100–106.
[3] K. Fujimoto, T. Oba, Appl. Catal. 13 (1985) 289–293.
[4] M. Inoue, T. Miyake, Y. Takegami, T. Inui, Appl. Catal. 29 (1987) 285–294.
[5] T. Tatsumi, A. Muramatsu, T. Fukunaga, H. Tominaga, Proc. 9th Int. Congr. on Catalysis, vol. 2, 1988, pp. 618–625.
[6] C.B. Murchison, M.M. Conway, R.R. Stevens, G.J. Quarderer, Proc. 9th Int. Congr. on Catalysis, vol. 2, 1988, pp. 626–633.
[7] R.G. Herman, Stud. Surf. Sci. Catal. 64 (1991) 266–349.
[8] Z. Li, Y. Fu, J. Bao, M. Jiang, T. Hu, T. Liu, Y. Xie, Appl. Catal. A: Gen. 220 (1) (2001) 21–30.
[9] D. Li, C. Yang, H. Qi, H. Zhang, W. Li, Y. Sun, B. Zhong, Catal. Commun. 5 (2004) 605–609.
[10] J. Iranmahboob, D.O. Hill, Catal. Lett. 78 (1–4) (2002) 49–55.
[11] P. Forzatti, E. Tronconi, I. Pasquon, Catal. Rev.-Sci. Eng. 33 (1991) 109–168.
[12] A.B. Stiles, F. Chen, J.B. Harrison, X. Hu, D.A. Storm, H.X. Yang, Ind. Eng. Chem. Res. 30 (1991) 811–821.
[13] J.C. Slaa, J.G. van Ommen, J.R.H. Ross, Catal. Today 15 (1992) 129–148.
[14] K.P. de Jong, J.W. Geus, Catal. Rev. Sci. Eng. 42 (4) (2000) 481–510.
[15] P. Serp, M. Corrias, P. Kalck, Appl. Catal. A: Gen. 253 (2003) 337–358.
[16] H.B. Zhang, G.D. Lin, Y.Z. Yuan, Curr. Top. Catal. 4 (2005) 1–21.
[17] H.B. Zhang, X.L. Liang, X. Dong, H.Y. Li, G.D. Lin, Catal. Surv. Asia 13 (1) (2009) 41–58.
[18] S. Iijima, Nature 354 (1991) 56–58.
[19] J.M. Planeix, N. Coustel, B. Coq, V. Brotons, P.S. Kumbhar, R. Dutartre, P. Geneste, P. Bernier, P.M. Ajiayan, J. Am. Chem. Soc. 116 (1994) 7935–7936.
[20] M.S. Hoogenraad, M.F. Onwezen, A.J. van Dillen, J.W. Geus, Stud. Surf. Sci. Catal. 101 (1996) 1331–1339.
[21] Y. Zhang, H.-B. Zhang, G.-D. Lin, P. Chen, Y.-Z. Yuan, K.-R. Tsai, Appl. Catal. A: Gen. 187 (1999) 213–224.
[22] J.Z. Luo, L.Z. Gao, Y.L. Leung, C.T. Au, Catal. Lett. 66 (2000) 91–97.
[23] H.-B. Chen, J.-D. Lin, Y. Cai, X.-Y. Wang, J. Yi, J. Wang, G. Wei, Y.-Z. Lin, D.-W. Liao, Appl. Surf. Sci. 180 (2001) 328–330.
[24] Z.-J. Liu, Z.-D. Xu, Z.-Y. Yuan, D.-Y. Lu, W.-X. Chen, W.-Z. Zhou, Catal. Lett. 72 (2001) 203–206.
[25] E. van Steen, F.F. Prinsloo, Catal. Today 71 (2002) 327–334.
[26] H.-B. Zhang, X. Dong, G.-D. Lin, Y.-Z. Yuan, P. Zhang, K.-R. Tsai, in: C.J. Liu, R.G. Mallinson, M. Aresta (Eds.), Utilization of Greenhouse Gases, ACS Symp. Ser., vol. 852, 2003, pp. 195–209.
[27] X. Dong, H.-B. Zhang, G.-D. Lin, Y.-Z. Yuan, K.-R. Tsai, Catal. Lett. 85 (2003) 237–246.
[28] H.-B. Zhang, X. Dong, G.-D. Lin, X.-L. Liang, H.-Y. Li, Chem. Commun. (40) (2005) 5094–5096.
[29] X.-M. Ma, G.-D. Lin, H.-B. Zhang, Catal. Lett. 111 (2006) 141–151.
[30] X.-L. Pan, Z.-L. Fan, W. Chen, Y.-J. Ding, H.-Y. Luo, X.-H. Bao, Nat. Mater. 6 (2007) 507–511.
[31] X.-M. Wu, Y.-Y. Guo, J.-M. Zhou, G.-D. Lin, X. Dong, H.-B. Zhang, Appl. Catal. A: Gen. 340 (2008) 87–97.
[32] X. Dong, X.-L. Liang, H.-Y. Li, G.-D. Lin, P. Zhang, H.-B. Zhang, Catal. Today 147 (2) (2009) 158–165.
[33] X.-L. Liang, X. Dong, G.-D. Lin, H.-B. Zhang, Appl. Catal. B: Environ. 88 (3–4) (2009) 315–322.
[34] P. Chen, H.-B. Zhang, G.-D. Lin, Q. Hong, K.-R. Tsai, Carbon 35 (10–11) (1997) 1495–1501.
[35] L.K. Kurihara, G.M. Chow, P.E. Schoen, NanoStruct. Mater. 5 (1995) 607–613.
[36] P. Chen, H.-B. Zhang, G.-D. Lin, K.-R. Tsai, Chem. J. Chin. Univ. 19 (5) (1998) 765–769.
[37] J.-M. Zhou, Y. Wang, P.-P. Tang, X.-M. Wu, G.-D. Lin, H.-B. Zhang, Chin. J. Appl. Chem. 22 (2) (2005) 117–122.
[38] H.-B. Zhang, G.-D. Lin, Z.-H. Zhou, X. Dong, T. Chen, Carbon 40 (2002) 2429–2436.
[39] XRD data bank attached to X'Pert PRO X-ray Diffractometer, PANalytical, The Netherlands, 2003.
[40] J.F. Moulder, W.F. Stickle, P.E. Sobol, K.D. Bomben, Handbook of X-ray photoelectron spectroscopy—A Reference Book of Standard Spectra for Identification and Interpretation of XPS Data, Physical Electronics Inc., Eden Prairie, MN, USA, 1995.
[41] J. Abart, E. Delgado, G. Ertl, H. Jeziorowshi, H. Knözinger, N. Thiele, X.Z. Wang, E. Taglauer, Appl. Catal. 2 (1982) 155–176.
[42] A.M. Venezia, Catal. Today 77 (2003) 359–370.
[43] H.-B. Zhang, G.L. Schrader, J. Catal. 99 (2) (1986) 461–471.
[44] H.-B. Zhang, Y. Zhang, G.-D. Lin, Y.-Z. Yuan, K.-R. Tsai, Stud. Surf. Sci. Catal. 130, Proc. 12th Intern. Congr. on Catal., vol. D, 2000, pp. 3885–3890.
[45] H.D. Kaesz, R.B. Saillant, Chem. Rev. 72 (3) (1972) 231.
[46] B.F.G. Johnson, J. Lewis, Adv. Inorg. Chem. Radiochem. 24 (1981) 261.
[47] N.N. Kavtaradze, N.P. Sokolova, Russian J. Phys. Chem. 44 (1970) 1485.
[48] H.-B. Chen, Y.-Y. Liao, H.-B. Zhang, K.R. Tsai, Chin. Chem. Lett. 4 (5) (1993) 457–458.
[49] Y. Ishikawa, L.G. Austin, D.E. Brown, P.L. Walker Jr., P.L. Walker Jr., in: P.L. Walker Jr., P.A. Thrower (Eds.), Chemistry and Physics of Carbon, vol. 12, American Carbon Society, Marcel Dekker, New York, 1975, pp. 39–139.
[50] Z.-H. Zhou, X.-M. Wu, Y. Wang, G.-D. Lin, H.-B. Zhang, Acta Phys.-Chim. Sin. 18 (8) (2002) 692–698.